

# UC Berkeley

## UC Berkeley Previously Published Works

**Title**

Effects of Surface Roughness on the Electrochemical Reduction of CO<sub>2</sub> over Cu

**Permalink**

<https://escholarship.org/uc/item/1b87t8zf>

**Journal**

ACS Energy Letters, 5(4)

**ISSN**

2380-8195

**Authors**

Jiang, K  
Huang, Y  
Zeng, G  
[et al.](#)

**Publication Date**

2020-04-10

**DOI**

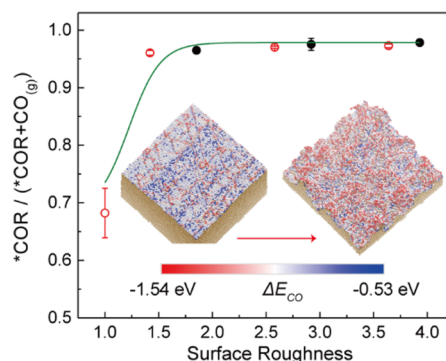
10.1021/acsenergylett.0c00482

Peer reviewed

# Effects of Surface Roughness on the Electrochemical Reduction of CO<sub>2</sub> over Cu

Kun Jiang,<sup>▽</sup> Yufeng Huang,<sup>▽</sup> Guosong Zeng, Francesca M. Toma, William A. Goddard, III, and Alexis T. Bell<sup>\*</sup>

**ABSTRACT:** We have investigated the role of surface roughening on the CO<sub>2</sub> reduction reaction (CO<sub>2</sub>RR) over Cu. The activity and product selectivity of Cu surfaces roughened by plasma pretreatment in Ar, O<sub>2</sub>, or N<sub>2</sub> were compared with that of electrochemically polished Cu samples. Differences in total and product current densities, the ratio of current densities for HER (the hydrogen evolution reaction) to CO<sub>2</sub>RR, and the ratio of current densities for C<sub>2+</sub> to C<sub>1</sub> products depend on the electrochemically active surface and are nearly independent of plasma composition. Theoretical analysis of an electropolished and roughened Cu surface reveals a higher fraction of undercoordinated Cu sites on the roughened surface, sites that bind CO preferentially. Roughened surfaces also contain square sites similar to those on a Cu(100) surface but with neighboring step sites, which adsorb OC–COH, a precursor to C<sub>2+</sub> products. These findings explain the increases in the formation of oxygenates and hydrocarbons relative to CO and the ratio of oxygenates to hydrocarbons observed with increasing surface roughness.



Electrochemical CO<sub>2</sub> reduction reaction (CO<sub>2</sub>RR) offers a promising route for the production of chemicals and fuels using renewable electricity generated from wind and solar energy.<sup>1–4</sup> Among metallic electrocatalysts evaluated for this purpose, copper is the only metal that produces hydrocarbons and oxygenated products with high Faradaic efficiency (FE).<sup>5–10</sup> Previous studies have shown that the activity and selectivity of Cu are strongly dependent on the surface morphology of the metal, as well as its local reaction environment (electrolyte composition and pH).<sup>11–16</sup> For example, Cu(100) and Cu(211) surfaces are more active than Cu(111) surfaces and more effective in promoting C–C bond formation on both single-crystal Cu electrodes<sup>17,18</sup> and Cu nanoparticles.<sup>19,20</sup> Recent theoretical calculations have shown that square sites of Cu(100) bind \*OCCO and \*OCCHO more strongly than do sites on Cu(111) and that the step sites of Cu(211) facilitate the kinetics of CO dimerization relative to those on Cu(111), resulting in a higher C<sub>2+</sub>/C<sub>1</sub> selectivity on square and stepped facets.<sup>21,22</sup> The role of other low-coordination Cu sites beyond those present on low-index facets is the subject of continuing discussion. An investigation of the CO<sub>2</sub>RR over size-controlled Cu nanoparticles has also shown that the population of low-coordination Cu surface sites increases with decreasing Cu particle size (from 15 to 2 nm) and that low coordination sites result in higher H<sub>2</sub> and CO selectivities and lower hydrocarbon (CH<sub>4</sub> and C<sub>2</sub>H<sub>4</sub>) selectivities.<sup>23</sup> By contrast, a comparative investigation of

CO<sub>2</sub>RR on (100)-, (111)-, and (751)-preferentially orientated Cu thin-film electrodes revealed that both Cu(100) and (751) surfaces with Cu coordination numbers from 6 to 8 promote C–C bond formation relative to more highly coordinated sites on Cu(111) surfaces.<sup>24</sup> More recently, a study of the electrochemical reduction of CO has suggested that highly porous Cu electrode could favor C<sub>2+</sub> oxygenates selectivity with a large suppression of competitive HER; however, the underlying causes for these observations remains unclear.<sup>25</sup>

Oxide-derived Cu with enriched surface grain boundaries have also been reported to be efficient for reducing CO<sub>2</sub> to multicarbon products.<sup>26–29</sup> It has been hypothesized that this enhanced C<sub>2+</sub> product selectivity on oxide-derived Cu could arise from surface Cu<sup>+</sup> retained under reaction conditions and stabilized by subsurface oxygen<sup>28,30</sup> or adsorbed halide anions,<sup>31,32</sup> e.g., I<sup>–</sup>, based on *quasi in situ* spectroscopic experiments. However, this hypothesis has been challenged by recent DFT calculations,<sup>33,34</sup> <sup>18</sup>O labeling,<sup>35</sup> electrochemical Raman spectroscopy,<sup>36,37</sup> and *in situ* synchrotron XAS and XRD experiments,<sup>38,39</sup> suggesting the near-surface oxygen and/or

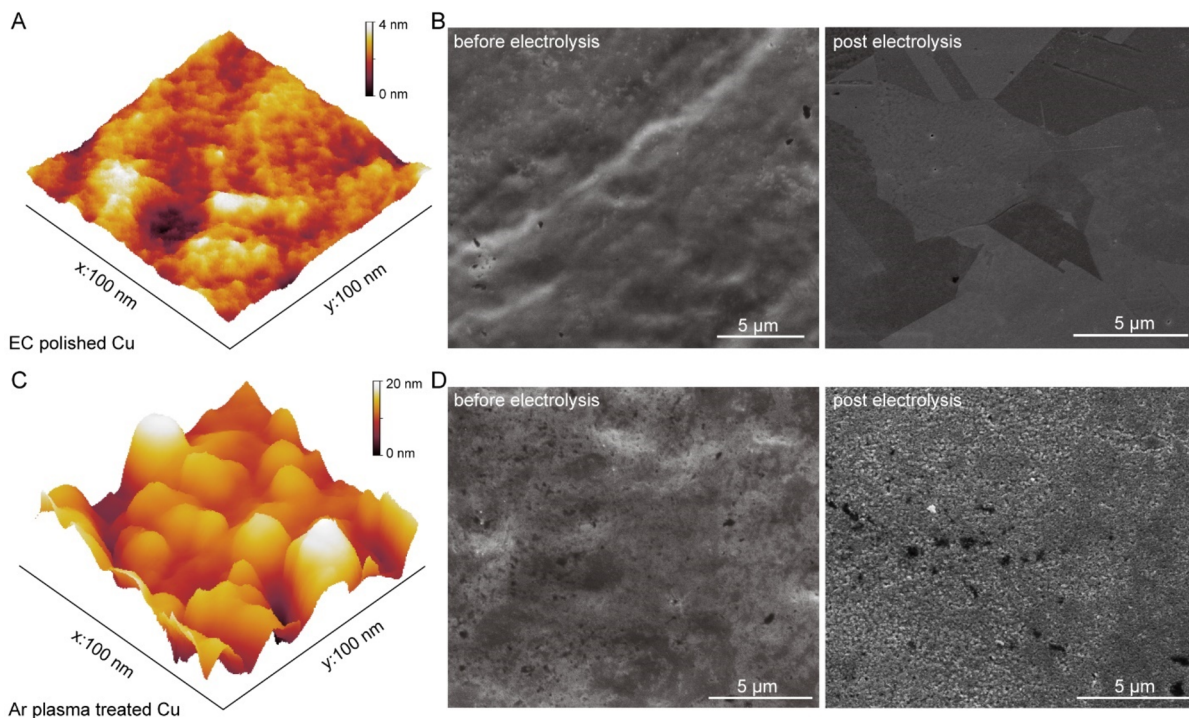


**Figure 1.** Cu electrodes characterization. AFM and SEM images of electrochemically polished Cu foil acquired before (A and B) and after a 10 min plasma pretreatment in Ar (C and D). Images A and C show the reconstructed 3D topography of the surface obtained from AFM scans; images B and D show typical SEM images of Cu foils taken before and after 1 h CO<sub>2</sub>RR electrolysis at  $-1.0$  V in CO<sub>2</sub>-saturated 0.1 M CsHCO<sub>3</sub>.

**Table 1.** Determined Surface Roughness of Post Electrolysis Cu Foils with Different Plasma Pretreatments

electrode	electropolished	N <sub>2</sub> plasma		Ar plasma		O <sub>2</sub> plasma		
		10 min	5 min	10 min	20 min	5 min	10 min	20 min
roughness	1.00	1.57	1.46	2.58	3.60	1.91	2.92	3.93

Cu(I) species are not sufficiently long-lived to be present under reaction conditions at highly reducing cathode potentials.<sup>40</sup> A more plausible interpretation for the enhanced C<sub>2+</sub> selectivity of oxide-derived Cu is offered by a recent theoretical analysis of sites present on a rough Cu nanoparticle. This work concludes that surface twin boundaries in the oxide-derived Cu associated with concave defects with respect to Cu(100) planes serve as active sites for C–C bond formation by stabilizing OC–COH species, one of the precursors to C<sub>2+</sub> products.<sup>41</sup>

In this study, we investigate the effects of plasma pretreatment of polished Cu foils in different gas atmospheres on their CO<sub>2</sub>RR activity and selectivity. Because O<sub>2</sub>-plasma treatment will cause both chemical and physical modifications to Cu surfaces, we pretreated Cu by Ar<sup>+</sup> ion bombardment in an Ar plasma in order to isolate the effects of surface roughening. These studies show that the changes in the distribution of CO<sub>2</sub>RR products is attributable to changes in Cu surface topography created by the plasma pretreatments. Roughened Cu surfaces containing a high proportion of under-coordinated Cu sites that exhibit stronger CO adsorption energies than more highly coordinated sites present of planar surfaces. Consistent with this finding, the fraction of CO formed from CO<sub>2</sub> released as CO decreases and the fraction converted to hydrocarbons and alcohols increases with increasing roughness. Our experimental efforts are supported by an analysis of the distribution of sites on a simulated roughened surface of Cu. This work shows that the roughened surface contains a much higher proportion of under-coordinated sites, and in particular sites that adsorb OCCOH, a

suggested precursor to C<sub>2+</sub> products,<sup>41</sup> more strongly than do the more highly coordinated sites present on a Cu(100) surface.

*Surface Characterization before and after Plasma Pretreatment.* Panels A and B of Figure 1 show atomic force microscopy (AFM) and scanning electron microscopy (SEM) images, respectively, of the electrochemically polished Cu foil. Figure 1C presents the AFM topography image of Cu foil after 10 min of Ar plasma treatment. In contrast to the polished foil, the Ar plasma-treated foil is much rougher, exhibiting extensive ridges and valleys.<sup>42</sup> The arithmetic surface roughness factor (*S<sub>a</sub>*) increases from 1.28 nm for the electropolished foil to 7.68 nm after Ar<sup>+</sup> sputtering based on an AFM scan of a 500 × 500 nm<sup>2</sup> area (Figure S1). SEM images of Ar plasma treated Cu foil before and after CO<sub>2</sub>RR electrolysis are shown in Figure 1D. In agreement with the topography determined by AFM, the 2D projection exhibits a surface structure covered with pits and islands generated by Ar<sup>+</sup> bombarding and redeposition of Cu atoms. Similar surface roughening effects were also observed for N<sub>2</sub> and O<sub>2</sub> plasma-treated Cu foils (Figure S2).

To further quantify the surface roughness of Cu foil electrodes, we determined the electrochemically active surface area (ECSA) by measuring the double-layer capacitances and then calculating the relative roughness of plasma-pretreated Cu compared to electropolished Cu (Table 1 and Figure S3). In general, all of the plasma treatments increased the roughness of Cu, and prolonged pretreatment time led to a more roughened surface. For the same pretreatment duration, Cu foils treated in either an Ar or O<sub>2</sub> plasma were rougher than that exposed to an

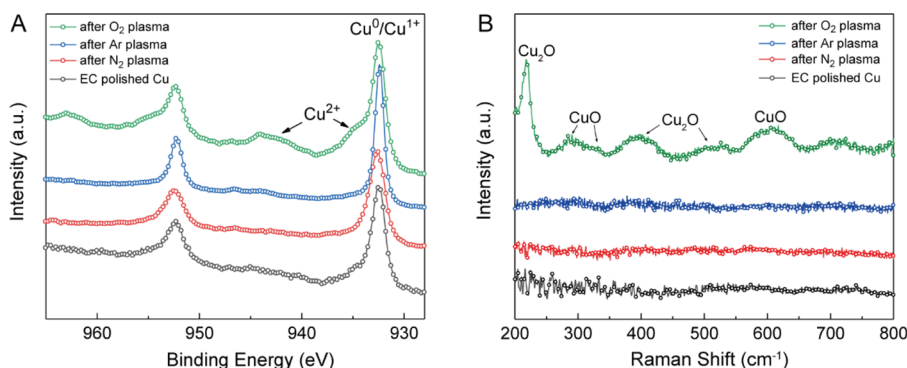


Figure 2. Chemical state characterization of Cu electrodes. *Ex situ* (A) XPS and (B) Raman spectra recorded on Cu foils after 10 min plasma treatments under different gaseous atmospheres.

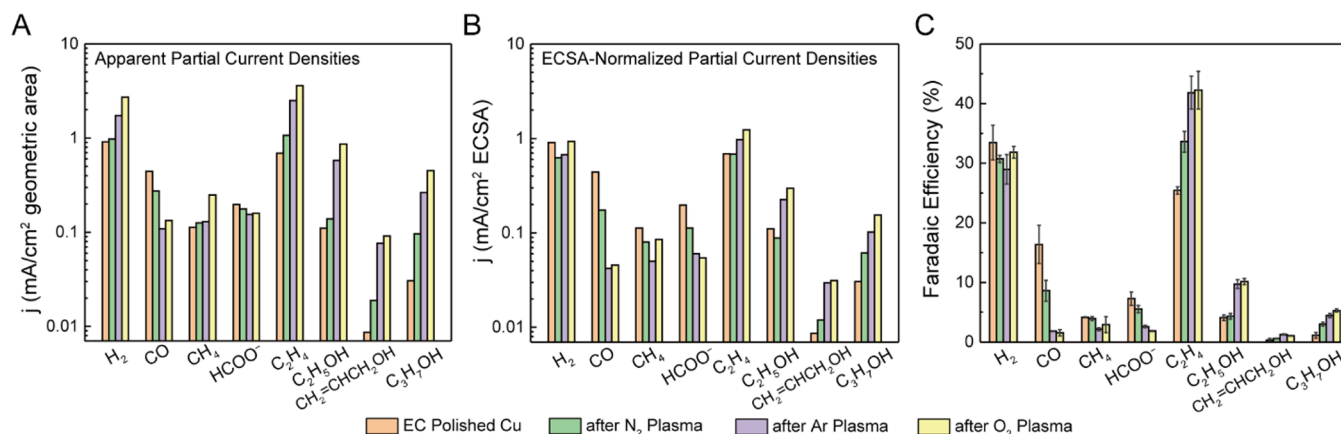


Figure 3. Electrochemical reduction of  $\text{CO}_2$  over Cu foil electrodes after 10 min plasma pretreatments under different gaseous atmospheres. (A) Geometric area normalized, (B) ECSA-normalized partial current densities, and (C) selectivity of major products during  $\text{CO}_2\text{RR}$  over Cu foil electrodes after 10 min of plasma pretreatments under different atmosphere.

$\text{N}_2$  plasma. These differences are likely due to the larger ion size of  $\text{Ar}^+$ , the more aggressive etching of  $\text{O}^{2-}$ ,<sup>43,44</sup> as well as the pronounced surface structural rearrangement caused by removal of oxygen from copper oxide during electrochemical reduction.<sup>26,34</sup> We also note that plasma pretreatment in an  $\text{N}_2$  plasma for more than 10 min did not increase the surface roughness of Cu further, in contrast to what was observed for pretreatment in an  $\text{O}_2$  plasma.

Figure 2A shows the *ex situ* core-level X-ray photoelectron spectra (XPS) of the Cu 2p region after plasma treatments in different atmospheres. All four samples show the predominant peak at 932.4 (Cu  $2p_{3/2}$ ) and 952.2 eV (Cu  $2p_{1/2}$ ), corresponding to Cu(0) or Cu(I). For the  $\text{O}_2$  plasma-treated Cu, two other satellite peaks show up at  $\sim 935$  and  $\sim 944$  eV, which are assigned to Cu(II) species. Evidence for Cu(II) cation was also obtained from the Cu LMM region of the Auger spectrum (see Figure S4). Raman spectra of these four Cu samples are shown in Figure 2B. No obvious Raman scattering feature is observed for electropolished Cu or Cu exposed to an  $\text{N}_2$  or Ar plasma. By contrast, features for both  $\text{Cu}_2\text{O}$  ( $\sim 218$ , 402, and 526  $\text{cm}^{-1}$ ) and  $\text{CuO}$  ( $\sim 290$ , 332, and 617  $\text{cm}^{-1}$ ) are observed after  $\text{O}_2$  plasma pretreatment,<sup>45</sup> in agreement with XPS spectra and Raman studies reported previously.<sup>28,32</sup>

**Electrochemical Activity and Selectivity.** The electrochemical  $\text{CO}_2\text{RR}$  performance of plasma-pretreated Cu foils was evaluated by 1 h chronoamperometric electrolysis at  $-1.0$  V vs RHE, for which the  $\text{CO}_2$  consumption rate is below 17.0  $\text{nmol s}^{-1} \text{cm}^{-2}$  (Figure S5).<sup>46</sup> The 0.1 M  $\text{CsHCO}_3$  was employed as

the supporting electrolyte, based upon our previous studies showing that  $\text{Cs}^+$  cations enhance the field stabilization of the intermediates critical to the formation  $\text{C}_2$  products<sup>13,14,47</sup> (further evidence for influence of cation identity is given in Figure S6). The superficial current densities shown in Figure 3A all increase with plasma pretreatment, in the order of the increasing ECSA. To account for this effect, Figure 3B shows the current densities for all four samples normalized by the ECSA. The ECSA-normalized current densities for  $\text{H}_2$  and  $\text{CH}_4$  are not strongly changed by plasma pretreatment, whereas those for CO and  $\text{HCOO}^-$  decreases and those for all  $\text{C}_{2+}$  product increases in the order no pretreatment <  $\text{N}_2$  plasma pretreatment < Ar plasma pretreatment <  $\text{O}_2$  plasma pretreatment. We note in particular that the rate of CO evolution decreases by more than an order of magnitude upon Ar or  $\text{O}_2$  plasma-pretreated Cu compared to that for electropolished Cu, and the rate of  $\text{C}_3$  products generation—allyl alcohol and *n*-propanol—increases by a factor of 3–5. The FEs of the principal products of the  $\text{CO}_2\text{RR}$  generated on electropolished and plasma pretreated Cu are illustrated in Figure 3C. After 10 min of plasma pretreatment, the selectivity toward hydrogen evolution (HER) and methane generation does not change very much, while the FEs for CO and  $\text{HCOO}^-$  decrease in the order of polished Cu >  $\text{N}_2$  plasma pretreated Cu > Ar plasma pretreated Cu  $\approx$   $\text{O}_2$  plasma pretreated Cu. By contrast, the FEs for  $\text{C}_{2+}$  products— $\text{C}_2\text{H}_4$ ,  $\text{C}_2\text{H}_5\text{OH}$ , and *n*-propanol—follow the reverse trend.

The similarity of both  $\text{C}_{2+}$  product selectivities and specific activities of Cu after Ar or  $\text{O}_2$  pretreatment is particularly



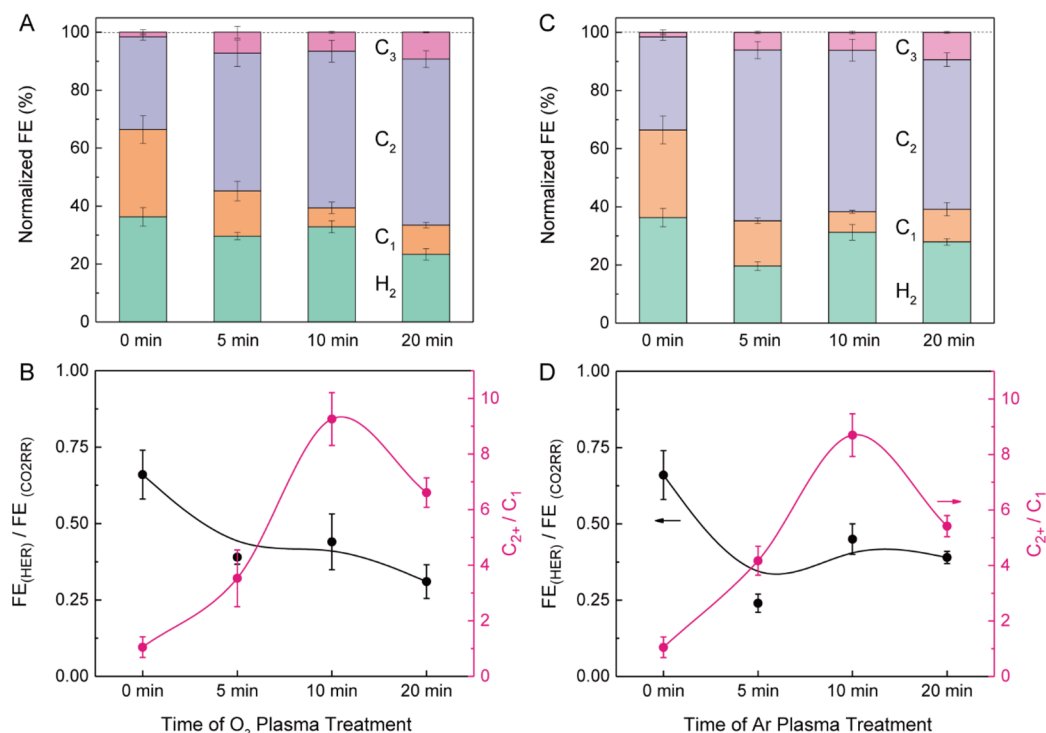


**Figure 4.** CO<sub>2</sub>RR products distribution as a function of plasma treatment time. Both (A and B) O<sub>2</sub> and (C and D) Ar atmosphere plasma pretreatments were plotted. The sum of as-determined overall FEs are varied from 92.2% to 98.9% and all normalized to 100% in panels A and C for comparison.

interesting. Therefore, we investigated the effects of the duration of plasma pretreatment in Ar and O<sub>2</sub> on the distribution of CO<sub>2</sub>RR products. Figure 4 shows these results for durations of 0, 5, 10, and 20 min, with the electropolished sample referenced as 0 min. The normalized FEs (referenced to 100%) are given in Figure 4A,C. The FE for HER is the cyan column, the FE for C<sub>1</sub> products (HCOO<sup>-</sup>, CO and CH<sub>4</sub>) the orange column, the FE for C<sub>2</sub> products (C<sub>2</sub>H<sub>4</sub> and C<sub>2</sub>H<sub>5</sub>OH) the purple column, and the FE for C<sub>3</sub> products (allyl alcohol and *n*-propanol) the magenta column. The selectivity ratio of HER/CO<sub>2</sub>RR (black line) and the C<sub>2</sub><sup>+</sup>/C<sub>1</sub> ratio (red line) are illustrated in Figure 4B,D. We observe similar product distributions throughout the time-course for both O<sub>2</sub> and Ar plasma pretreatments, which could largely rule out the (sub)surface oxygen effect. HER decreases to below 30% after 5 min of plasma exposure in both cases and levels off with prolonged exposure. The FE for C<sub>1</sub> products also decreases from 0 to 10 min, and it then increases again because of enhanced methane evolution after a 20 min pretreatment. Over the same pretreatment time, the FE for C<sub>3</sub> alcohols reaches ~10%, whereas the FE for C<sub>2</sub><sup>+</sup> products rises to ~60%. The ratio of C<sub>2</sub><sup>+</sup>/C<sub>1</sub> reaches a maximum value of ~9 after 10 min of pretreatment in either an Ar or O<sub>2</sub> plasma.

Because the Cu surface roughness increases with prolonged plasma-treatment time, we assessed whether the changes shown in Figure 4 correlate with surface roughness. The choice of which product ratios to plot is guided by recent theoretical studies of the CO<sub>2</sub>RR mechanism, which suggest that 2e<sup>-</sup> products (HCOO<sup>-</sup> and CO<sub>g</sub>) are produced via the adsorbed intermediates \*HCOO and \*COOH, respectively, whereas both CH<sub>4</sub> and C<sub>2</sub><sup>+</sup> products are produced via the reduction of \*CO.<sup>5,6,48–51</sup> Therefore, as illustrated in Figure 5A, \*CO serves as the key intermediate to CH<sub>4</sub> and C<sub>2</sub><sup>+</sup> products. Panels B and C of Figure 5 plot the selectivity ratios for C<sub>2</sub><sup>+</sup> products versus C<sub>1</sub>

products (HCOO<sup>-</sup>, CO, and CH<sub>4</sub>) and versus CH<sub>4</sub> alone, respectively. The C<sub>2</sub><sup>+</sup>/C<sub>1</sub> ratio reaches a value of ~9 for a roughness of ~3 and then decreases thereafter, regardless of whether Cu is pretreated in an Ar or O<sub>2</sub> plasma. By contrast, the C<sub>2</sub><sup>+</sup>/CH<sub>4</sub> ratio increases monotonically to a value of 30 in the case of Ar plasma pretreatment but reaches a maximum value of ~20 and then decreases in the case of O<sub>2</sub> pretreatment.

Figure 5D shows that the fraction of CO produced by the CO<sub>2</sub>RR converted to CH<sub>4</sub> and C<sub>2</sub><sup>+</sup> products increases from 0.68 for a roughness of 1.0 to 0.96 for a roughness of 1.5. Further increasing the roughness to ~4.0 increases this ratio to 0.98. The trend observed in Figure 5D suggests that the binding energy for CO increases monotonically with surface roughness, consistent with temperature-programmed desorption experiments<sup>26</sup> and recent theoretical calculations on simulated Cu particle surface.<sup>41,52</sup> The theoretical work also predicts that the stability of \*OC–COH, a critical precursor to C<sub>2</sub> products, increases with surface roughness and in particular with the formation of concave sites at grain boundaries between Cu(100) and Cu(111) surfaces. The downturn in the ratio of FEs for C<sub>2</sub><sup>+</sup> product formation and CH<sub>4</sub> formation seen in Figure 5C when the roughness exceeds ~3.0 for O<sub>2</sub> plasma pretreated Cu might be attributable to the formation of subnanometric Cu clusters (i.e., surface dimer and trimer adatoms) that could serve as active sites for selective CO<sub>2</sub>-to-CH<sub>4</sub> conversion.<sup>53</sup> Finally, Figure 5E shows the surface roughness dependence of the ratio of FEs for C<sub>2</sub><sup>+</sup> oxygenated products to that for C<sub>2</sub><sup>+</sup> hydrocarbons. The selectivity to C<sub>2</sub><sup>+</sup> oxygenated products (ethanol, allyl alcohol, and *n*-propanol) increases by a factor of 2 with increasing roughness, most likely because of the lower surface coverage by \*H, as reflected in the HER trend of Figure 4, and the reduced likelihood of hydrogenating C–C intermediates on the roughened Cu surfaces. Similarly, the selectivity to HCOO<sup>-</sup>

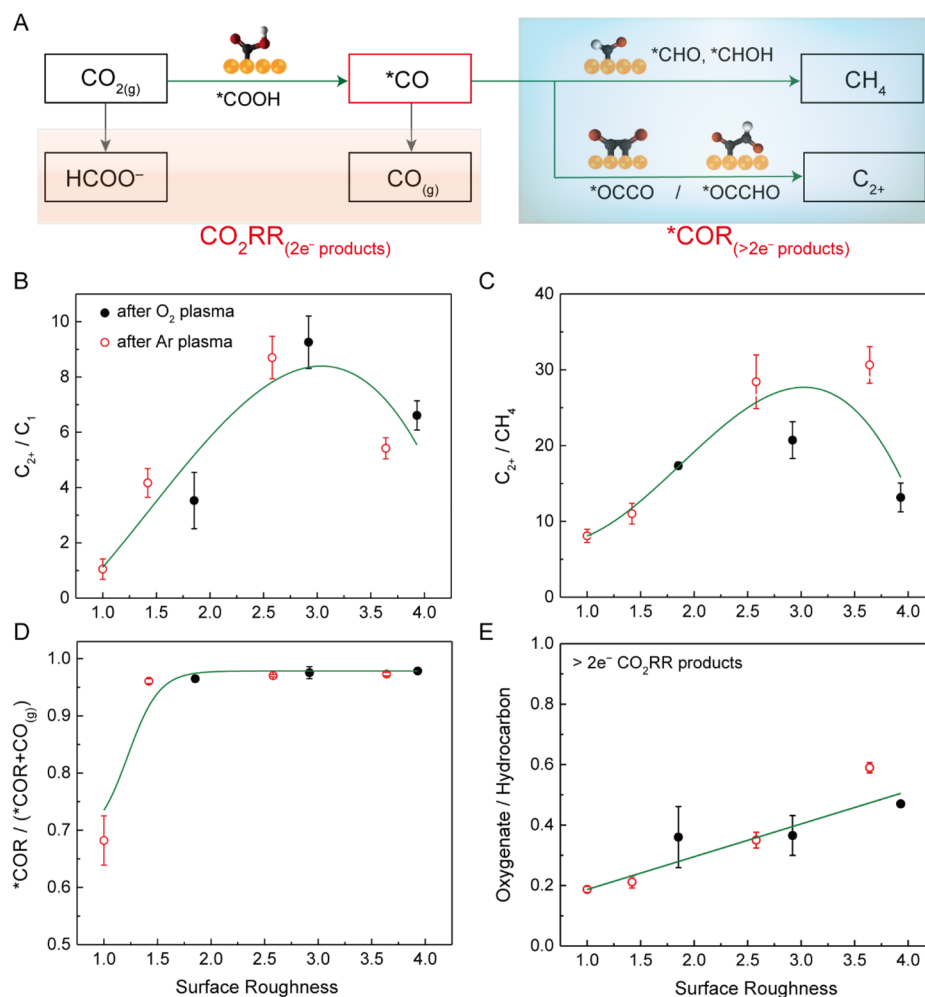


**Figure 5.** CO<sub>2</sub>RR products distribution as a function of Cu surface roughness. (A) Simplified flowchart of CO<sub>2</sub>RR mechanism leading to C<sub>1</sub> and C<sub>2+</sub> product generation. \* corresponds to adsorbed species, > 2e<sup>-</sup> reduction products of CH<sub>4</sub> and C<sub>2+</sub> that go through the reduction of \*CO intermediate (\*COR) are marked in light blue. (B) C<sub>2+</sub>/C<sub>1</sub> ratio, (C) C<sub>2+</sub>/C<sub>CH<sub>4</sub></sub> ratio, (D) \*COR/(CO<sub>(g)</sub> + \*COR) ratio, and (E) oxygenate/hydrocarbon (only >2e<sup>-</sup> reduction products) ratio.

decreases as the roughness increases from 1.0 to 2.6 and levels off thereafter (Figure S7). We suggest that this trend is due to the lower availability of terrace sites on roughened Cu surfaces, which are needed to bond bidentate \*HCOO, the precursor to HCOOH and hence HCOO<sup>-</sup> upon desorption of HCOOH into the alkaline electrolyte.<sup>6</sup>

A further factor that can contribute to enhancing the ratio of C<sub>2+</sub>/CH<sub>4</sub> on roughened versus smooth Cu surfaces is the higher local pH near the surface of the roughened Cu; therefore, we considered the possible effect of pH on the observed results. The higher pH near the roughened surface can be ascribed to the higher rate of OH<sup>-</sup> generation rate per geometric electrode area. We note that this proposal is consistent with the control experiment presented in Figure S8, illustrating the effects of increased bicarbonate concentration, and the earlier findings of Hori et al., who reported a 4-fold enhancement in the C<sub>2+</sub>/CH<sub>4</sub> ratio upon increasing the surface pH from 8.5 to 9.5.<sup>54</sup> In our studies, we observed only a ~2.6-fold increase in the C<sub>2+</sub>/CH<sub>4</sub> ratio because of an estimated increase in the surface pH change from 9.76 to 9.88 for Cu treated for 5 min versus 10 min in an Ar plasma. The pH for these experiments was estimated assuming a mass-transfer boundary layer thickness of ~40 μm and a bicarbonate concentration of 0.1 M.<sup>46,55</sup> We also note that it has

been reported that the increase in surface pH as a consequence of electrolyte polarization should suppress CH<sub>4</sub> production but keep C<sub>2+</sub> activity constant at a given potential.<sup>56,57</sup> Figure 3B shows that while the intrinsic activity (ECSA-normalized partial current density) for forming CH<sub>4</sub> decreases following plasma pretreatment, the intrinsic activities for producing C<sub>2+</sub> products, especially oxygenated products, increases. These observations suggest that the enhanced C<sub>2+</sub> selectivity observed after plasma treatment is not attributable to the small change in the local pH.

Table S1 compares our results on the effects of surface roughness with those previously reported. Various methods have been used to roughen the surface of Cu. These include reduction of copper oxides produced by thermal and/or plasma oxidation, potential cycling in halogen-containing solutions, dendrite growth, etc. Regardless of the method used to achieve roughening, increased surface roughness generally leads to an enhanced C<sub>2+</sub> FE and C<sub>2+</sub>/C<sub>1</sub> ratio. Most authors have attributed these effects of enhanced surface roughness to a greater abundance of under-coordinated surface sites and defective sites that bind \*CO strongly and promote its further reduction to C–C bond formation. Unfortunately, these results cannot be compared with those reported here because of the

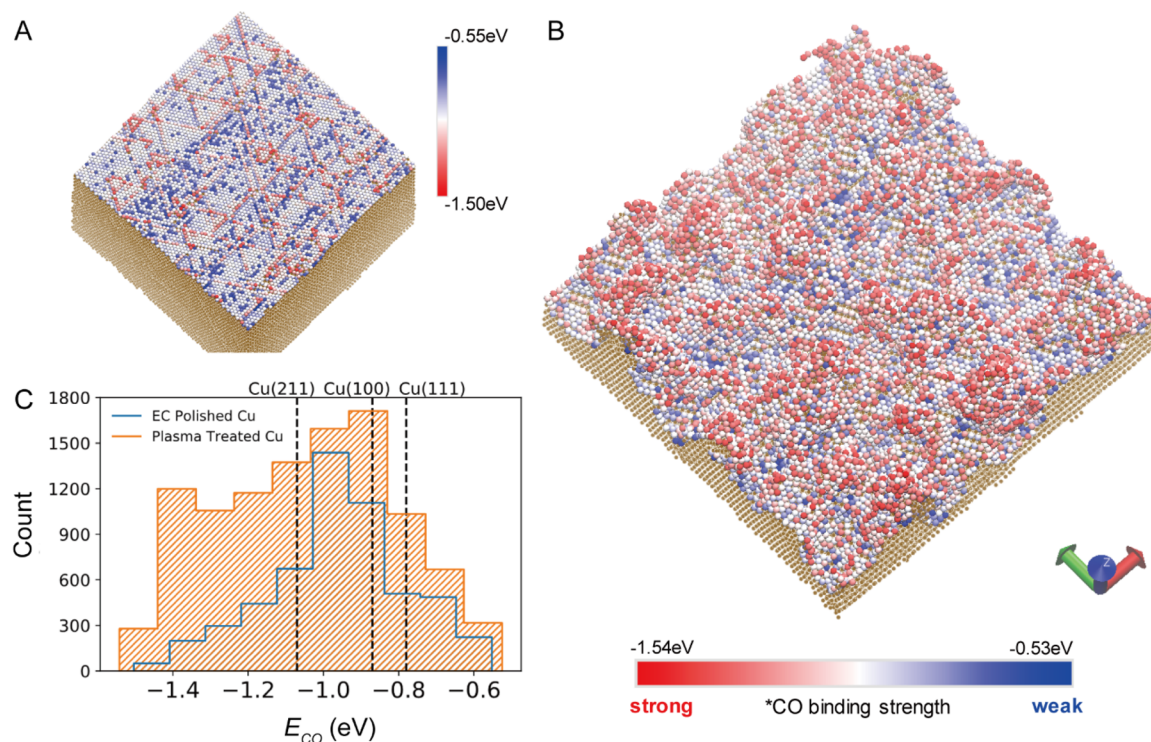


**Figure 6. Active site visualization by ReaxQM-Machine Learning.** Images of the computationally produced Cu surface of (A) electro-polished and (B) after Ar plasma bombardment and (C) predicted distribution of CO adsorption energies,  $\Delta E_{\text{CO}}$ . The three dashed lines indicate the CO adsorption energies on Cu(111), (100), and (211).

large difference in the modes of sample preparation and conditions for their investigation.

**Theoretical Simulation and Analysis.** Insights into why surface roughening causes an increase in the formation of  $\text{C}_{2+}$  products can be gained by atomic-level analysis of the Cu surface created by computational simulation of  $\text{Ar}^+$  bombardment roughening of a Cu(111) surface followed by thermal relaxation of the resulting surface. The simulation of roughening begins with a  $17.6 \times 17.4 \text{ nm}^2$  surface that is 10.1 nm thick, which contains  $\sim 5422$  total surface atoms (see Figure 6A). Figure 6B and the Supporting Movie 1 show that after bombardment of this surface with 1300  $\text{Ar}^+$  cations, the Cu surface exposes 10 433 atoms, corresponding to an increase in surface roughness of 1.93. The simulated untreated Cu surface and the plasma-treated surface resemble the topography and roughness of the experimental observations, as seen in Figure 1.

The ReaxQM-Machine Learning approach was used to predict the distribution of CO binding energies,  $\Delta E_{\text{CO}}$ , for both simulated electrochemically polished Cu and the Ar plasma roughened surfaces.<sup>41,58</sup> The electropolished Cu, shown in Figure 6A, is dominated by close-packed low index sites, and therefore, the mean values of  $\Delta E_{\text{CO}}$  are close to those of Cu(111), (100), and (211) surfaces (Figure 6C). By contrast, a much higher population of stronger CO binding sites, ranging from  $-1.10$  to  $-1.54 \text{ eV}$  (red sites along the ridges in Figure 6B and the columns left of the Cu(211) line in Figure 6C), appear after plasma pretreatment. The increased number of strong CO binding sites is consistent with the experimental observation of a reduced selectivity to CO formation following plasma pretreatment to roughen the catalyst surface. Because the adsorption of  $\text{*CO}$  and  $\text{*H}$  are expected to compete on the surface of Cu, the stronger adsorption of CO on roughened Cu is expected to result in a reduction of the  $\text{*H}/\text{*CO}$ . This reasoning would

explain the increase in the formation of oxygenated relative to hydrocarbon products observed with increasing roughening seen in Figure 5E.

In our previous work we have employed the formation energy of  $\text{*OC-COH}$  ( $\Delta E_{\text{OCCOH}}$ ) as a descriptor for the selectivity of  $\text{C}_{2+}$  products formed during the  $\text{CO}_2\text{RR}$  and have shown that the mean value of  $\Delta E_{\text{OCCOH}}$  decreased from  $\sim 1.35 \text{ eV}$  for random surface sites to  $\sim 0.50 \text{ eV}$  for surface square sites.<sup>39</sup> We also noted that concave defects located at the Cu(100) plane next to a (111) step exhibited the most favorable values of  $\Delta E_{\text{OCCOH}}$  for  $\text{C}_{2+}$  selectivity. In the present study, we identified the surface square sites on the simulated Cu surfaces for comparison, as shown in Figure 7A,B. The percentage of square sites to overall surface atoms increased from 20.9% on the polished Cu surface to 38.5% on the surface produced by Ar plasma pretreatment. Figure 7C shows the atomic structures of randomly chosen square sites occurring on the simulated surface produced by plasma treatment. The sites are similar to the Cu(100) configuration but have abundant neighboring step sites. As noted, the significantly increased percentage of surface square sites favors C–C bond formation and provides a rational for the enhanced  $\text{C}_{2+}$  selectivity that correlates with increased surface roughening caused by plasma pretreatment.

In conclusion, the present study investigated the effects of surface topography on the activity and product selectivity of electrochemical  $\text{CO}_2$  reaction, demonstrating the distribution of products produced by  $\text{CO}_2\text{RR}$  on metallic Cu changes with Cu surface topography created by plasma pretreatment. The activity and product selectivity of electrochemically polished Cu was compared with those of roughened Cu surfaces prepared by different plasma pretreatments. The differences in overall  $\text{CO}_2\text{RR}$  activity from different plasma pretreatments are attributable to changes in the electrochemically active surface



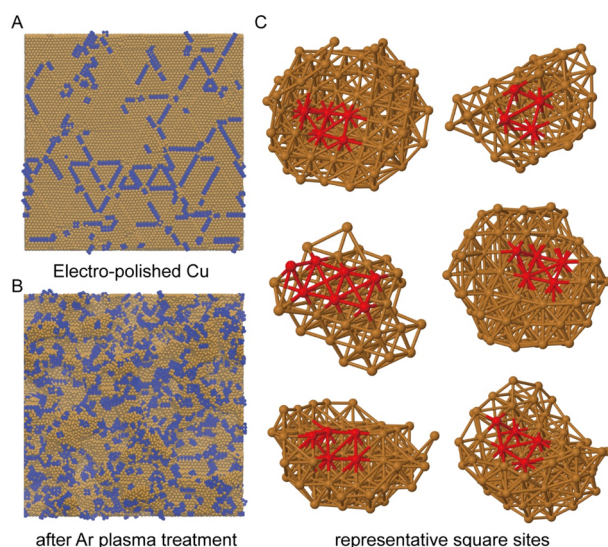


**Figure 7. Visualization of square sites on computationally simulated Cu surfaces.** (A) Electropolished Cu and (B) Ar plasma pretreated Cu. The surface square sites are marked in blue. (C) Zoomed-in atomic structure of randomly chosen square sites on the plasma-treated Cu surface, both the square sites and the neighboring Cu step sites (if any) are highlighted in red.

area. Of particular note, we observe that with increasing surface roughness, the ratio of current densities for  $\text{CO}_2\text{RR}$  to HER, the ratio of the current densities for COR to the sum of the current densities for CO formation and COR, and the ratio of current densities for formation oxygenates to hydrocarbons all increase. These trends are interpreted based on an atomic-level analysis of the topography of roughened Cu surface. We find that CO formed by the electrochemical reduction of  $\text{CO}_2$  binds more strongly on the roughened surface than on the electrochemically polished surface, suggesting that the ratio of adsorbed H to CO decreases with increasing surface roughness. These trends explain why the fraction of CO produced by  $\text{CO}_2$  reduction converted to reduced products and the fraction of these products appearing as oxygenates rather than hydrocarbons increase with increasing surface roughness. A further effect of increasing surface roughness is an increase in the fraction of final products (oxygenates and hydrocarbons) containing two or more C atoms. Our analysis shows that surface roughening increases the fraction of square sites similar to those on a Cu(100) surface but having abundant neighboring step sites. Prior work has shown that such sites enhance the formation of C–C bonds required to form  $\text{C}_{2+}$  products during the electrochemical reduction of  $\text{CO}_2$ . Finally, we find that increased roughening of the Cu surface increases the ratio of current densities for  $\text{C}_{2+}$  to  $\text{C}_1$  (CO,  $\text{HCOO}^-$ , and  $\text{CH}_4$ ) products up to a maximum value of  $\sim 9$  for a surface roughness of  $\sim 3$ . Most of this downturn is ascribed to the enhanced formation of  $\text{CH}_4$  on surfaces with roughness in excess of 3. The enhanced formation of methane on highly roughened surfaces is attributed to the formation of surface dimer and trimer clusters on the Cu surface that have been shown by theoretical calculation to serve as active sites for selective conversion of  $\text{CO}_2$  to  $\text{CH}_4$ . In summary, the results of the present work highlight the importance of surface topography and defect sites on the observed  $\text{CO}_2$  reduction activity and selectivity and suggest that rational surface structure engineering could contribute to the development of Cu

electrocatalysts exhibiting a high selectivity to multicarbon products.

### Supporting Information

The Supporting Information is available free of charge at <https://pubs.acs.org/doi/10.1021/acsenergylett.0c00482>.

Experimental and computational details; additional Cu electrode characterization by AFM, SEM, Auger, XPS, and electrochemical double-layer capacitance measurements; Cu surface roughness dependence of  $\text{CO}_2$  consumption rate and  $\text{FE}_{\text{formate}}/\text{FE}_{(\text{CO}+\text{COR})}$  ratio during chronoamperometric electrolysis; online differential electrochemical mass spectrometry study on the cation effect; control experiments study on anion buffering effect and extra surface roughening at the presence of iodide anion (PDF)

Supporting Movie 1: Cu surface after Ar plasma bombardment (MP4)

## AUTHOR INFORMATION

### Corresponding Author

Alexis T. Bell — Joint Center for Artificial Photosynthesis and Chemical Sciences Division, Lawrence Berkeley National Laboratory, Berkeley, California 94720, United States; Department of Chemical and Biomolecular Engineering, University of California, Berkeley, California 94720, United States; [orcid.org/0000-0002-5738-4645](https://orcid.org/0000-0002-5738-4645); Email: [alexbell@berkeley.edu](mailto:alexbell@berkeley.edu)

### Authors

Kun Jiang — Institute of Fuel Cells, School of Mechanical Engineering, Shanghai Jiao Tong University, Shanghai 200240, China; Joint Center for Artificial Photosynthesis, Lawrence Berkeley National Laboratory, Berkeley, California 94720, United States; Department of Chemical and Biomolecular Engineering, University of California, Berkeley, California 94720, United States; [orcid.org/0000-0003-3148-5058](https://orcid.org/0000-0003-3148-5058)

Yufeng Huang — Materials Simulation Center and Joint Center for Artificial Photosynthesis, California Institute of Technology, Pasadena, California 91125, United States

Guosong Zeng — Chemical Sciences Division, Lawrence Berkeley National Laboratory, Berkeley, California 94720, United States  
Francesca M. Toma — Joint Center for Artificial Photosynthesis and Chemical Sciences Division, Lawrence Berkeley National Laboratory, Berkeley, California 94720, United States; [orcid.org/0000-0003-2332-0798](https://orcid.org/0000-0003-2332-0798)

William A. Goddard, III — Materials Simulation Center and Joint Center for Artificial Photosynthesis, California Institute of Technology, Pasadena, California 91125, United States; [orcid.org/0000-0003-0097-5716](https://orcid.org/0000-0003-0097-5716)

Complete contact information is available at: <https://pubs.acs.org/doi/10.1021/acsenergylett.0c00482>

### Author Contributions

<sup>†</sup>K.J. and Y.H. contributed equally to this work.

### Notes

The authors declare no competing financial interest.

## ACKNOWLEDGEMENTS

This material is based upon work performed by the Joint Center for Artificial Photosynthesis, a DOE Energy Innovation Hub,



supported through the Office of Science of the U.S. Department of Energy under Award Number DE-SC0004993. K.J. acknowledges the startup funding from Shanghai Jiao Tong University. We also acknowledge Ms. Lien-Chun Weng, Dr. Zhou Lin, and Prof. Martin Head-Gordon for insightful discussions.

## REFERENCES

- (1) De Luna, P.; Hahn, C.; Higgins, D.; Jaffer, S. A.; Jaramillo, T. F.; Sargent, E. H. What would it take for renewably powered electrosynthesis to displace petrochemical processes? *Science* **2019**, *364* (6438), No. eaav3506.
- (2) Shih, C. F.; Zhang, T.; Li, J.; Bai, C. Powering the Future with Liquid Sunshine. *Joule* **2018**, *2* (10), 1925–1949.
- (3) Jouny, M.; Luc, W.; Jiao, F. General Techno-Economic Analysis of CO<sub>2</sub> Electrolysis Systems. *Ind. Eng. Chem. Res.* **2018**, *57* (6), 2165–2177.
- (4) Verma, S.; Kim, B.; Jhong, H.; Ma, S. C.; Kenis, P. J. A. A Gross-Margin Model for Defining Technoeconomic Benchmarks in the Electroreduction of CO<sub>2</sub>. *ChemSusChem* **2016**, *9* (15), 1972–1979.
- (5) Hori, Y.; Wakebe, H.; Tsukamoto, T.; Koga, O. Electrocatalytic Process of Co Selectivity in Electrochemical Reduction of CO<sub>2</sub> at Metal-Electrodes in Aqueous-Media. *Electrochim. Acta* **1994**, *39* (11–12), 1833–1839.
- (6) Kortlever, R.; Shen, J.; Schouten, K. J. P.; Calle-Vallejo, F.; Koper, M. T. M. Catalysts and Reaction Pathways for the Electrochemical Reduction of Carbon Dioxide. *J. Phys. Chem. Lett.* **2015**, *6* (20), 4073–4082.
- (7) Zhu, D. D.; Liu, J. L.; Qiao, S. Z. Recent Advances in Inorganic Heterogeneous Electrocatalysts for Reduction of Carbon Dioxide. *Adv. Mater.* **2016**, *28* (18), 3423–3452.
- (8) Xu, S.; Carter, E. A. Theoretical Insights into Heterogeneous (Photo)electrochemical CO<sub>2</sub> Reduction. *Chem. Rev.* **2019**, *119* (11), 6631–6669.
- (9) Gao, D.; Arán-Ais, R. M.; Jeon, H. S.; Roldan Cuenya, B. Rational catalyst and electrolyte design for CO<sub>2</sub> electroreduction towards multicarbon products. *Nat. Catal.* **2019**, *2* (3), 198–210.
- (10) Nitopi, S.; Bertheussen, E.; Scott, S. B.; Liu, X.; Engstfeld, A. K.; Horch, S.; Seger, B.; Stephens, I. E. L.; Chan, K.; Hahn, C.; Nørskov, J. K.; Jaramillo, T. F.; Chorkendorff, I. Progress and Perspectives of Electrochemical CO<sub>2</sub> Reduction on Copper in Aqueous Electrolyte. *Chem. Rev.* **2019**, *119* (12), 7610–7672.
- (11) Pérez-Gallent, E.; Marcandalli, G.; Figueiredo, M. C.; Calle-Vallejo, F.; Koper, M. T. M. Structure- and Potential-Dependent Cation Effects on CO Reduction at Copper Single-Crystal Electrodes. *J. Am. Chem. Soc.* **2017**, *139* (45), 16412–16419.
- (12) Kim, D.; Kley, C. S.; Li, Y.; Yang, P. Copper nanoparticle ensembles for selective electroreduction of CO<sub>2</sub> to C<sub>2</sub>–C<sub>3</sub> products. *Proc. Natl. Acad. Sci. U. S. A.* **2017**, *114* (40), 10560–10565.
- (13) Resasco, J.; Chen, L. D.; Clark, E.; Tsai, C.; Hahn, C.; Jaramillo, T. F.; Chan, K.; Bell, A. T. Promoter Effects of Alkali Metal Cations on the Electrochemical Reduction of Carbon Dioxide. *J. Am. Chem. Soc.* **2017**, *139* (32), 11277–11287.
- (14) Singh, M. R.; Kwon, Y.; Lum, Y.; Ager, J. W.; Bell, A. T. Hydrolysis of Electrolyte Cations Enhances the Electrochemical Reduction of CO<sub>2</sub> over Ag and Cu. *J. Am. Chem. Soc.* **2016**, *138* (39), 13006–13012.
- (15) Roberts, F. S.; Kuhl, K. P.; Nilsson, A. Electroreduction of Carbon Monoxide Over a Copper Nanocube Catalyst: Surface Structure and pH Dependence on Selectivity. *ChemCatChem* **2016**, *8* (6), 1119–1124.
- (16) Kas, R.; Kortlever, R.; Yilmaz, H.; Koper, M. T. M.; Mul, G. Manipulating the Hydrocarbon Selectivity of Copper Nanoparticles in CO<sub>2</sub> Electroreduction by Process Conditions. *ChemElectroChem* **2015**, *2* (3), 354–358.
- (17) Hori, Y.; Takahashi, I.; Koga, O.; Hoshi, N. Selective Formation of C<sub>2</sub> Compounds from Electrochemical Reduction of CO<sub>2</sub> at a Series of Copper Single Crystal Electrodes. *J. Phys. Chem. B* **2002**, *106* (1), 15–17.
- (18) Huang, Y.; Handoko, A. D.; Hirunsit, P.; Yeo, B. S. Electrochemical Reduction of CO<sub>2</sub> Using Copper Single-Crystal Surfaces: Effects of CO\* Coverage on the Selective Formation of Ethylene. *ACS Catal.* **2017**, *7* (3), 1749–1756.
- (19) Loiudice, A.; Lobaccaro, P.; Kamali, E. A.; Thao, T.; Huang, B. H.; Ager, J. W.; Buonsanti, R. Tailoring Copper Nanocrystals towards C-2 Products in Electrochemical CO<sub>2</sub> Reduction. *Angew. Chem., Int. Ed.* **2016**, *55* (19), 5789–5792.
- (20) Jiang, K.; Sandberg, R. B.; Akey, A. J.; Liu, X.; Bell, D. C.; Nørskov, J. K.; Chan, K.; Wang, H. Metal Ion Cycling of Cu Foil for Selective C-C Coupling in Electrochemical CO<sub>2</sub> Reduction. *Nat. Catal.* **2018**, *1*, 111–119.
- (21) Schouten, K. J. P.; Pérez Gallent, E.; Koper, M. T. M. Structure Sensitivity of the Electrochemical Reduction of Carbon Monoxide on Copper Single Crystals. *ACS Catal.* **2013**, *3* (6), 1292–1295.
- (22) Sandberg, R. B.; Montoya, J. H.; Chan, K.; Nørskov, J. K. CO-CO coupling on Cu facets: Coverage, strain and field effects. *Surf. Sci.* **2016**, *654*, 56–62.
- (23) Reske, R.; Mistry, H.; Behafarid, F.; Roldan Cuenya, B.; Strasser, P. Particle Size Effects in the Catalytic Electroreduction of CO<sub>2</sub> on Cu Nanoparticles. *J. Am. Chem. Soc.* **2014**, *136* (19), 6978–6986.
- (24) Hahn, C.; Hatsukade, T.; Kim, Y. G.; Vailionis, A.; Baricauatro, J. H.; Higgins, D. C.; Nitopi, S. A.; Soriaga, M. P.; Jaramillo, T. F. Engineering Cu surfaces for the electrocatalytic conversion of CO<sub>2</sub>: Controlling selectivity toward oxygenates and hydrocarbons. *Proc. Natl. Acad. Sci. U. S. A.* **2017**, *114* (23), 5918–5923.
- (25) Wang, L.; Nitopi, S.; Wong, A. B.; Snider, J. L.; Nielander, A. C.; Morales-Guio, C. G.; Orazov, M.; Higgins, D. C.; Hahn, C.; Jaramillo, T. F. Electrochemically converting carbon monoxide to liquid fuels by directing selectivity with electrode surface area. *Nat. Catal.* **2019**, *2* (8), 702–708.
- (26) Verdaguer-Casadevall, A.; Li, C. W.; Johansson, T. P.; Scott, S. B.; McKeown, J. T.; Kumar, M.; Stephens, I. E. L.; Kanan, M. W.; Chorkendorff, I. Probing the Active Surface Sites for CO Reduction on Oxide-Derived Copper Electrocatalysts. *J. Am. Chem. Soc.* **2015**, *137* (31), 9808–9811.
- (27) Ren, D.; Deng, Y. L.; Handoko, A. D.; Chen, C. S.; Malkhandi, S.; Yeo, B. S. Selective Electrochemical Reduction of Carbon Dioxide to Ethylene and Ethanol on Copper(I) Oxide Catalysts. *ACS Catal.* **2015**, *5* (5), 2814–2821.
- (28) Mistry, H.; Varela, A. S.; Bonifacio, C. S.; Zegkinoglou, I.; Sinev, I.; Choi, Y. W.; Kisslinger, K.; Stach, E. A.; Yang, J. C.; Strasser, P.; Cuenya, B. R. Highly selective plasma-activated copper catalysts for carbon dioxide reduction to ethylene. *Nat. Commun.* **2016**, *7*, 12123.
- (29) Lum, Y.; Yue, B.; Lobaccaro, P.; Bell, A. T.; Ager, J. W. Optimizing C–C Coupling on Oxide-Derived Copper Catalysts for Electrochemical CO<sub>2</sub> Reduction. *J. Phys. Chem. C* **2017**, *121* (26), 14191–14203.
- (30) Eilert, A.; Cavalca, F.; Roberts, F. S.; Osterwalder, J.; Liu, C.; Favaro, M.; Crumlin, E. J.; Ogasawara, H.; Friebe, D.; Pettersson, L. G. M.; Nilsson, A. Subsurface Oxygen in Oxide-Derived Copper Electrocatalysts for Carbon Dioxide Reduction. *J. Phys. Chem. Lett.* **2017**, *8* (1), 285–290.
- (31) Gao, D. F.; Zegkinoglou, I.; Divins, N. J.; Scholten, F.; Sinev, I.; Grosse, P.; Roldan Cuenya, B. Plasma-Activated Copper Nanocube Catalysts for Efficient Carbon Dioxide Electroreduction to Hydrocarbons and Alcohols. *ACS Nano* **2017**, *11* (5), 4825–4831.
- (32) Gao, D. F.; McCrum, I. T.; Deo, S.; Choi, Y. W.; Scholten, F.; Wan, W. M.; Chen, J. G. G.; Janik, M. J.; Roldan Cuenya, B. Activity and Selectivity Control in CO<sub>2</sub> Electroreduction to Multicarbon Products over CuO<sub>x</sub> Catalysts via Electrolyte Design. *ACS Catal.* **2018**, *8* (11), 10012–10020.
- (33) Garza, A. J.; Bell, A. T.; Head-Gordon, M. Is Subsurface Oxygen Necessary for the Electrochemical Reduction of CO<sub>2</sub> on Copper? *J. Phys. Chem. Lett.* **2018**, *9* (3), 601–606.
- (34) Fields, M.; Hong, X.; Nørskov, J. K.; Chan, K. Role of Subsurface Oxygen on Cu Surfaces for CO<sub>2</sub> Electrochemical Reduction. *J. Phys. Chem. C* **2018**, *122* (28), 16209–16215.

- (35) Lum, Y. W.; Ager, J. W. Stability of Residual Oxides in Oxide-Derived Copper Catalysts for Electrochemical CO<sub>2</sub> Reduction Investigated with O-18 Labeling. *Angew. Chem., Int. Ed.* **2018**, *57* (2), 551–554.
- (36) Kibria, M. G.; Dinh, C.-T.; Seifitokaldani, A.; De Luna, P.; Burdyny, T.; Quintero-Bermudez, R.; Ross, M. B.; Bushuyev, O. S.; García de Arquer, F. P.; Yang, P.; Sinton, D.; Sargent, E. H. A Surface Reconstruction Route to High Productivity and Selectivity in CO<sub>2</sub> Electroreduction toward C<sub>2+</sub> Hydrocarbons. *Adv. Mater.* **2018**, *30* (49), 1804867.
- (37) Mandal, L.; Yang, K. R.; Motapothula, M. R.; Ren, D.; Lobaccaro, P.; Patra, A.; Sherburne, M.; Batista, V. S.; Yeo, B. S.; Ager, J. W.; Martin, J.; Venkatesan, T. Investigating the Role of Copper Oxide in Electrochemical CO<sub>2</sub> Reduction in Real Time. *ACS Appl. Mater. Interfaces* **2018**, *10* (10), 8574–8584.
- (38) Farmand, M.; Landers, A. T.; Lin, J. C.; Feaster, J. T.; Beeman, J. W.; Ye, Y.; Clark, E. L.; Higgins, D.; Yano, J.; Davis, R. C.; Mehta, A.; Jaramillo, T. F.; Hahn, C.; Drisdell, W. S. Electrochemical flow cell enabling operando probing of electrocatalyst surfaces by X-ray spectroscopy and diffraction. *Phys. Chem. Chem. Phys.* **2019**, *21* (10), 5402–5408.
- (39) Scott, S. B.; Hogg, T. V.; Landers, A. T.; Maagaard, T.; Bertheussen, E.; Lin, J. C.; Davis, R. C.; Beeman, J. W.; Higgins, D.; Drisdell, W. S.; Hahn, C.; Mehta, A.; Seger, B.; Jaramillo, T. F.; Chorkendorff, I. Absence of Oxidized Phases in Cu under CO Reduction Conditions. *ACS Energy Lett.* **2019**, *4* (3), 803–804.
- (40) Lei, Q.; Zhu, H.; Song, K.; Wei, N.; Liu, L.; Zhang, D.; Yin, J.; Dong, X.; Yao, K.; Wang, N.; Li, X.; Davaasuren, B.; Wang, J.; Han, Y. Investigating the Origin of Enhanced C<sub>2+</sub> Selectivity in Oxide-/Hydroxide-Derived Copper Electrodes during CO<sub>2</sub> Electroreduction. *J. Am. Chem. Soc.* **2020**, *142* (9), 4213–4222.
- (41) Huang, Y.; Chen, Y.; Cheng, T.; Wang, L.-W.; Goddard, W. A. Identification of the Selective Sites for Electrochemical Reduction of CO to C<sub>2+</sub> Products on Copper Nanoparticles by Combining Reactive Force Fields, Density Functional Theory, and Machine Learning. *ACS Energy Lett.* **2018**, *3* (12), 2983–2988.
- (42) Tang, W.; Peterson, A. A.; Varela, A. S.; Jovanov, Z. P.; Bech, L.; Durand, W. J.; Dahl, S.; Norskov, J. K.; Chorkendorff, I. The importance of surface morphology in controlling the selectivity of polycrystalline copper for CO<sub>2</sub> electroreduction. *Phys. Chem. Chem. Phys.* **2012**, *14* (1), 76–81.
- (43) Chiang, C.-C.; Chen, M.-C.; Li, L.-J.; Wu, Z.-C.; Jang, S.-M.; Liang, M.-S. Effects of O<sub>2</sub>- and N<sub>2</sub>-plasma treatments on copper surface. *Jpn. J. Appl. Phys.* **2004**, *43* (11R), 7415.
- (44) Fatyeyeva, K.; Dahi, A.; Chappey, C.; Langevin, D.; Valleton, J.-M.; Poncin-Epaillard, F.; Marais, S. Effect of cold plasma treatment on surface properties and gas permeability of polyimide films. *RSC Adv.* **2014**, *4* (59), 31036–31046.
- (45) Deng, Y. L.; Handoko, A. D.; Du, Y. H.; Xi, S. B.; Yeo, B. S. In Situ Raman Spectroscopy of Copper and Copper Oxide Surfaces during Electrochemical Oxygen Evolution Reaction: Identification of Cu-III Oxides as Catalytically Active Species. *ACS Catal.* **2016**, *6* (4), 2473–2481.
- (46) Clark, E. L.; Resasco, J.; Landers, A.; Lin, J.; Chung, L.-T.; Walton, A.; Hahn, C.; Jaramillo, T. F.; Bell, A. T. Standards and Protocols for Data Acquisition and Reporting for Studies of the Electrochemical Reduction of Carbon Dioxide. *ACS Catal.* **2018**, *8* (7), 6560–6570.
- (47) Ringe, S.; Clark, E. L.; Resasco, J.; Walton, A.; Seger, B.; Bell, A. T.; Chan, K. Understanding cation effects in electrochemical CO<sub>2</sub> reduction. *Energy Environ. Sci.* **2019**, *12* (10), 3001–3014.
- (48) Peterson, A. A.; Abild-Pedersen, F.; Studt, F.; Rossmeisl, J.; Norskov, J. K. How copper catalyzes the electroreduction of carbon dioxide into hydrocarbon fuels. *Energy Environ. Sci.* **2010**, *3* (9), 1311–1315.
- (49) Garza, A. J.; Bell, A. T.; Head-Gordon, M. Mechanism of CO<sub>2</sub> Reduction at Copper Surfaces: Pathways to C<sub>2</sub> Products. *ACS Catal.* **2018**, *8* (2), 1490–1499.
- (50) Zheng, Y.; Vasileff, A.; Zhou, X.; Jiao, Y.; Jaroniec, M.; Qiao, S. Z. Understanding the Roadmap for Electrochemical Reduction of CO<sub>2</sub> to Multi-Carbon Oxygenates and Hydrocarbons on Copper-Based Catalysts. *J. Am. Chem. Soc.* **2019**, *141* (19), 7646–7659.
- (51) Malkani, A. S.; Dunwell, M.; Xu, B. Operando Spectroscopic Investigations of Copper and Oxide-Derived Copper Catalysts for Electrochemical CO Reduction. *ACS Catal.* **2019**, *9* (1), 474–478.
- (52) Cheng, T.; Xiao, H.; Goddard, W. A. Nature of the Active Sites for CO Reduction on Copper Nanoparticles; Suggestions for Optimizing Performance. *J. Am. Chem. Soc.* **2017**, *139* (34), 11642–11645.
- (53) Zhao, Z. L.; Chen, Z. Z.; Zhang, X.; Lu, G. Generalized Surface Coordination Number as an Activity Descriptor for CO<sub>2</sub> Reduction on Cu Surfaces. *J. Phys. Chem. C* **2016**, *120* (49), 28125–28130.
- (54) Hori, Y.; Murata, A.; Takahashi, R. Formation of hydrocarbons in the electrochemical reduction of carbon dioxide at a copper electrode in aqueous solution. *J. Chem. Soc., Faraday Trans. 1* **1989**, *85* (8), 2309–2326.
- (55) Weng, L. C.; Bell, A. T.; Weber, A. Z. Towards membrane-electrode assembly systems for CO<sub>2</sub> reduction: a modeling study. *Energy Environ. Sci.* **2019**, *12* (6), 1950–1968.
- (56) Hori, Y.; Takahashi, R.; Yoshinami, Y.; Murata, A. Electrochemical Reduction of CO at a Copper Electrode. *J. Phys. Chem. B* **1997**, *101* (36), 7075–7081.
- (57) Resasco, J.; Lum, Y.; Clark, E.; Zeledon, J. Z.; Bell, A. T. Effects of Anion Identity and Concentration on Electrochemical Reduction of CO<sub>2</sub>. *ChemElectroChem* **2018**, *5* (7), 1064–1072.
- (58) Chen, Y.; Huang, Y.; Cheng, T.; Goddard, W. A. Identifying Active Sites for CO<sub>2</sub> Reduction on Dealloyed Gold Surfaces by Combining Machine Learning with Multiscale Simulations. *J. Am. Chem. Soc.* **2019**, *141* (29), 11651–11657.